Materials Science and Engineering A 528 (2011) 2863–2869

Contents lists available at ScienceDirect

Materials Science and Engineering A

journal homepage: www.elsevier.com/locate/msea

Strain sensing behavior of electrically conductive fibers under large deformation

J.P. Wang [a], P. Xue [a,*], X.M. Tao [b]

[a] School of Aeronautics, Northwestern Polytechnical University, PR China
[b] Institute of Textiles and Clothing, The Hong Kong Polytechnic University, Hong Kong

ARTICLE INFO

Article history:
Received 15 September 2010
Received in revised form
14 December 2010
Accepted 15 December 2010
Available online 23 December 2010

Keywords:
Flexible strain sensors
Conductive fibers
Image processing
Modeling

ABSTRACT

Electrically conductive fiber/yarn/fabric is one of the promising materials as flexible conductive sensors because of their sensitivity to strain, temperature and humidity. Aiming at developing of effective flexible sensors, this study investigates experimentally the strain sensing behavior of PPy (polypyrrole)-coated Lycra fibers, showing that the electrically resistance of the conductive fibers changes with the deformation of fibers. The variation in electrically resistance is mainly related to the micro-cracks appearing on the fiber surface during deformation. Then, the effects of the characteristic parameters of the micro-cracks are studied statistically by means of image processing functions in MATLAB, and the governing parameters are determined. Based on the results, a model is built to describe the variation of electrical resistance by the parameters of the micro-cracks. The analytical results are compared with the experimental results, showing an acceptable agreement.

1. Introduction

In recent years, various flexible sensors have come into use, which cut down the structural restrictions of conventional sensors [1–3]. Their applications have been found in military [4,5], biomedical [6,7] and robotics [8].

The flexible sensors are known for their outstanding features, such as flexibility and wearability. As a category of the flexible sensors, the electrically conductive sensors have been investigated and developed to sense the strain, temperature and humidity, and so on. In Florida University, PPy-coated textile fabrics were prepared with varying surface resistivities and were used to detect the ammonia and acid directly by monitoring conductivity changes [9]. The textile garments with the elastic fabrics (Lycra) and electrically conductive elastomers (CEs), developed by Pisa University in Italy, were able to detect the posture and movement of human body [10]. The smart gloves were made to detect the movement of fingers by Tao's group [11]. So far, most of the publications are on the fabrication of electrically conductive fiber/yarn/fabrics, and some experimental work on their sensing behavior. Investigations on sensing mechanisms and the modeling of the strain sensing behavior are very limited.

Aiming at developing effective flexible sensors, this study investigates experimentally the strain sensing behavior of PPy-coated Lycra fibers and its sensing mechanisms. The characteristic parameters of the micro-cracks are studied statistically by means of image processing functions in MATLAB. The relationship between the strain sensing behavior and various characteristic parameters on the coating layer is established. This work will provide guidance for R&D of the flexible conductive sensors, especially in material selection and their fabrication.

2. Experimental

The Lycra fibers with linear density of 40 denier/5F were supplied from Sunikorn Knitters Limited (HK), and the pyrrole and ferric chloride hexahydrate ($FeCl_3{\cdot}6H_2O$) were purchased from Sigma–Aldrich Chemical Company.

The electrically conductive fibers were obtained by coating a layer of PPy on the Lycra fibers through the chemical vapor deposition technique. The details on the coating process can be found in references [12,13]. The thickness of coating layer is approximately 300 nm.

Tensile tests were conducted on an Instron mechanical testing system (Model 4466). The load and deformation were recorded during testing. Its electrical resistance was measured by the four-probe method with a Keithley 2010 multimeter. The experimental setup is shown in Fig. 1. The crosshead speed was 5 mm/min and the gage length was 60 mm. Five specimens were tested and the average value of resistance was taken. All electro-mechanical tests were carried out at room temperature (20 °C) and relative humidity of 65% RH.

The change of the fiber surface during deformation were observed in situ by means of a scanning electron microscopy (SEM, Lecia Steroscan 440) equipped with a Gatan microtest module. A

* Corresponding author at: School of Aeronautics, Northwestern Polytechnical University, 127 Youyi Xilu, 118 Mail Box, PR China. Tel.: +86 29 88494859; fax: +86 29 88494859.
E-mail address: p.xue@nwpu.edu.cn (P. Xue).

0921-5093/$ – see front matter © 2010 Elsevier B.V. All rights reserved.
doi:10.1016/j.msea.2010.12.057

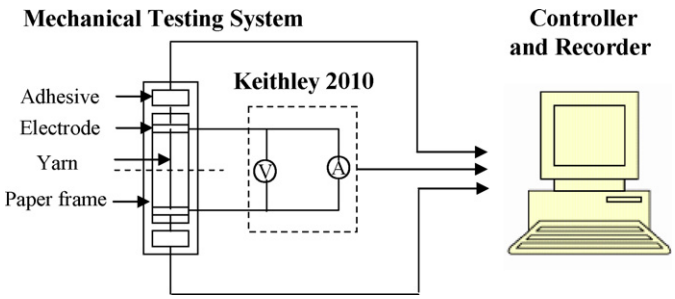

Fig. 1. Experimental setup of the tensile test.

small piece of yarn was fixed at the fixtures of the microtest and was loaded at a speed of 2 mm/min.

3. Results

Fig. 2 shows the relationship between the change of electrical resistance and the strain of the fibers obtained from tensile tests. It can be seen that electrical resistance increases nonlinearly with the strain, up to the strain of 0.5. At the beginning, the resistance increases slowly; after the strain of 0.2, there is an obvious change in electrical resistance.

The SEM microphotographs, obtained at the strain of 0, 0.06, 0.2, and 0.3, respectively, are shown in Fig. 3. From these images, it is evident that there were many micro-cracks occurring on the coating surface after being extended. This happened due to the much less elasticity of PPy than substrate fibers. From reference [14] it is known that larger difference between the Young's moduli of the PPy coating layer and the substrate will lead to cracks easily. All the micro-cracks were found transverse to mechanical stress and

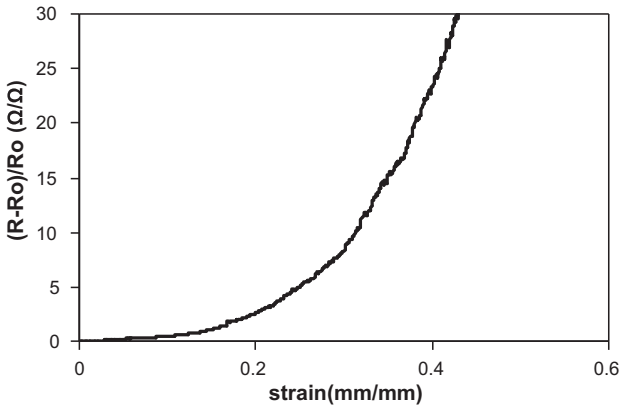

Fig. 2. Typical resistance vs. strain curve of PPy-coated Lycra fibers.

almost parallel to each other. Meanwhile, the cracks propagated during the deformation. The characteristics of the micro-cracks can be identified by the parameters, such as crack number, width and length. All these information can be abstracted from the SEM microphotographs by an image processing technique described in the next section.

4. Microscopic image processing technique

The image processing technique in this study can be summarized in a flow chart, shown in Fig. 4. The main procedures consist of seven steps, e.g. noise filtering, image binarization, image cropping, morphological opening operation, image thinning and skeleton extraction, identification of micro-cracks parameters, and pixel calibration.

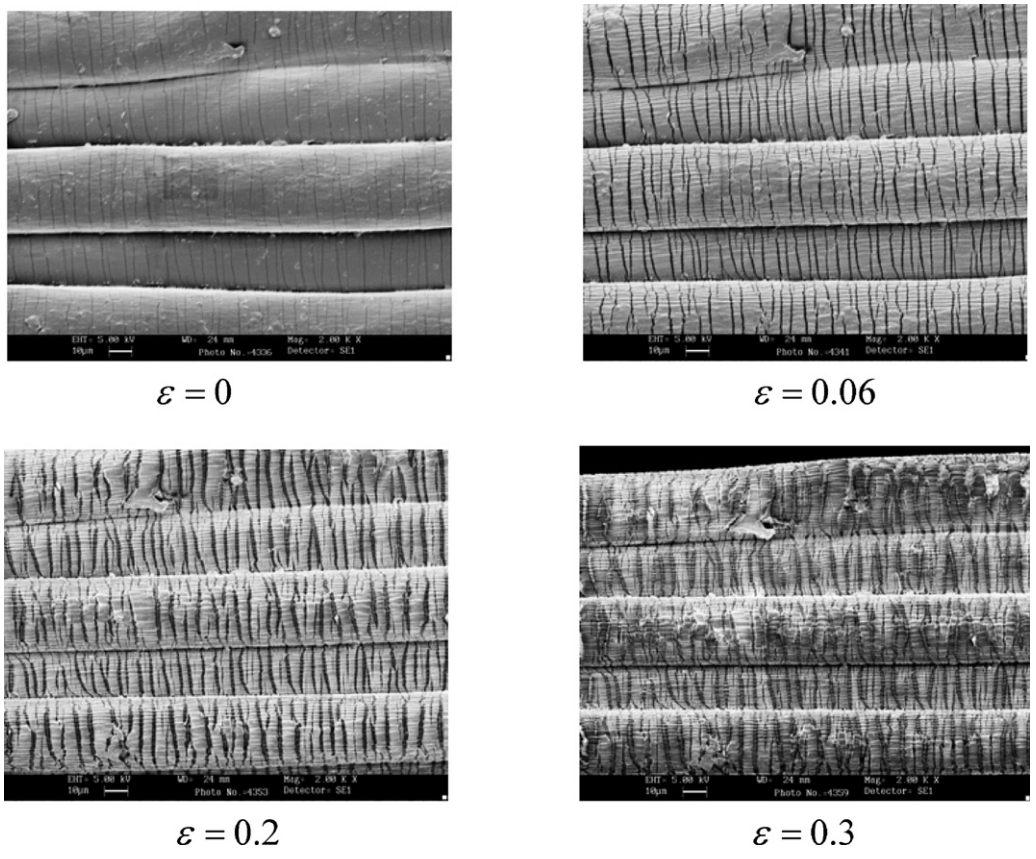

Fig. 3. SEM microphotographs of PPy-coated Lycra fibers at different strain level.

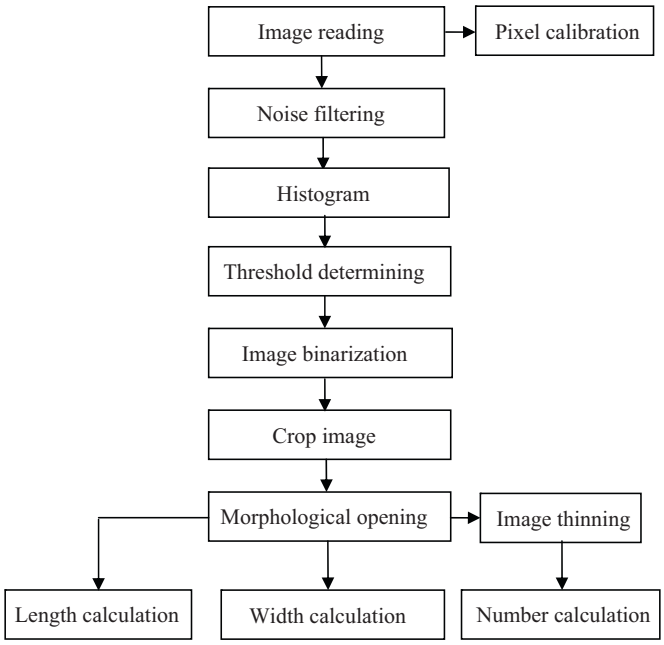

Fig. 4. Flow chart of image processing technique.

4.1. Noise filtering

The image contains inevitably noises because of the influence of testing environment, consequently affecting the statistical accuracy. However, the noise can be eliminated by filtering functions in image processing, so as to improve the image quality and highlight the image features.

"Median Filtering" is a nonlinear operation in image processing, usually being used to reduce "salt and pepper" noise. It means replacing the value of a pixel by the median of the gray levels in the neighborhood of the pixel, i.e.:

$$\hat{f}(x, y) = \underset{(s,t)\in S_{xy}}{\text{median}}\{g(s, t)\} \quad (1)$$

"Wiener Filtering" is a method which can implement the minimization of the mean square error of initial and target images [15]. Wiener 2, a filtering function in MATLAB, applies a pixelwise adaptive Wiener method based on statistics estimation from a local neighborhood of each pixel. For SEM microphotographs shown in Fig. 3, "Median Filtering" and "Wiener Filtering" are used to eliminate the image noises and to improve the image quality.

4.2. Image binarization

Generally, the images from experiments are grayscale, so they must be converted into binary images for further analysis. The so-called binary image is to change the grayscale image (grayscale from 0 to 255) into image with only two gray values (0 and 1). The latter is visually black and white image. The number "1" indicates that the pixel is at the prospect and the number "0" is at the

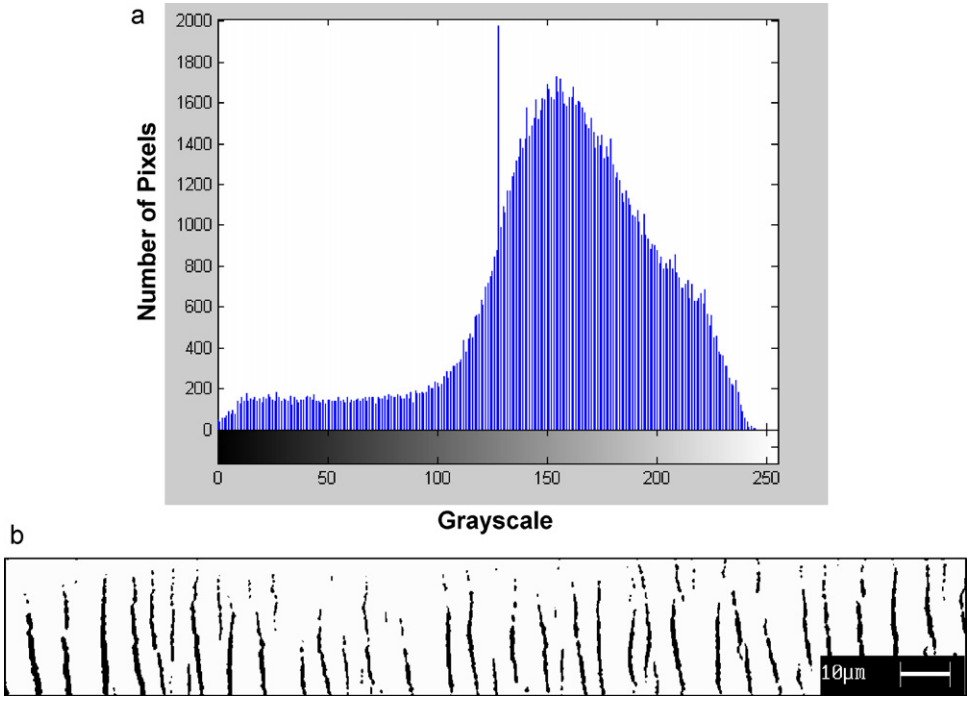

Fig. 5. (a) Histogram of the SEM grayscale image and (b) the corresponding binary image.

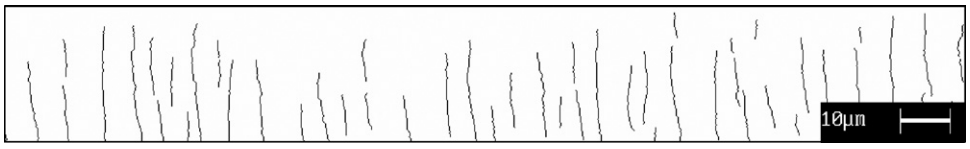

Fig. 6. Skeleton of the image.

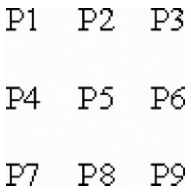

Fig. 7. Sub-matrix taken from binary image for counting micro-cracks.

background. Therefore, it is easier to identify the features of the image composition. In order to obtain characteristic parameters of micro-cracks more clearly and accurately, it is necessary to set the threshold, so as to distinguish the target (micro-cracks) from the background. It has been known that there are two ways to segment the image with the threshold, i.e. automatic segmentation and manual segmentation [16]. If the histogram has two peaks, the threshold will be set automatically; otherwise the threshold will be set manually. In this study, the histograms of the SEM images obtained from the experiment had a single peak (shown in Fig. 5(a)), so the images will be binarized by setting threshold manually as shown in Fig. 5(b).

4.3. Crop the image and remove background noise

A representative fiber is taken and its image is processed using MATLAB functions so as to obtain the parameters of micro-cracks. The "Imcrop" function in MATLAB is used to crop the rectangular area of one fiber. Then the "Morphological Opening" operation is applied to clear the false information in the area.

4.4. Image thinning and skeleton extraction

The skeleton of an image is obtained by thinning process in MATLAB, thus the number of the micro-cracks within a given surface area can be obtained in Section 4.5. The so-called thinning process is to abstract an outline of the binary image and replace the image by a skeleton which consists of cracks, while each crack is represented by one pixel width. The skeleton extraction is also defined as the medial axis transformation or prairie fire concept. The medial axis is the trajectory of the centers of circles which tangent with the two or more non-adjacent boundary points of the objects [15,17]. The medial axis can be found by skeletonizing function in MATLAB. By image thinning and skeleton extraction process for Fig. 5(b), the skeleton is obtained and shown in Fig. 6.

4.5. Characteristic parameters of the micro-cracks

The micro-cracks on the skeleton can be counted to obtain the number of micro-cracks in a given area referring to literatures. An algorithm proposed in [18] was used to get the number of cracks for the case that cracks distribute randomly, while the method given in [19] was to get the crack number on the surface of a corn where there were limited cracks on the surface. Both cases are different from our experimental observation. Therefore, a revised algorithm is proposed in this study and is given as follows.

It is known that the binary image is saved in a form of matrix during the image processing. Taking an arbitrary line in the binary image skeleton shown in Fig. 6, corresponding a row in the matrix, the black pixels (micro-cracks) can be searched in the matrix. Once one black pixel is found, assuming to be the element P5 in Fig. 7, its adjacent eight elements (P1, P2, P3, P4, P6, P7, P8, and P9) should be examined. If the gray values of two elements are zero, we can consider there is one crack. If the gray values of three elements are zero we think the crack has a bifurcation and the crack number is 2. By taking sufficient lines and processing in the same way, then taking a mean value, the number of micro-cracks in a selected image area can be obtained.

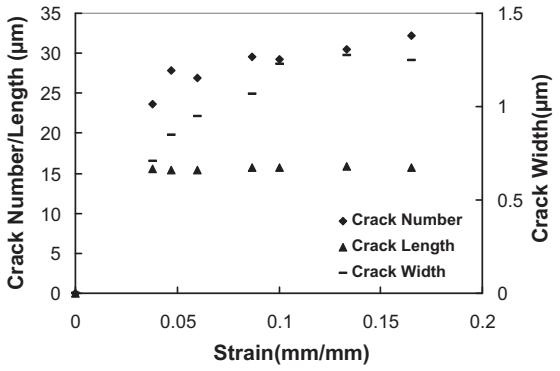

Fig. 8. Variation of the micro-cracks parameters with the strain.

Just like the method mentioned above, the total width of cracks in one line is obtained by searching the black pixels in a line of the binary image without thinning, and then divided by the number of micro-cracks, the width of the micro-cracks can be determined approximately. Assuming S is the number of total pixels in the selected image area, the length of cracks L' can be expressed as

$$L' = \frac{S}{N \cdot W} \tag{2}$$

where N and W are the number and width of the micro-cracks, respectively.

4.6. Pixel calibration

The length and the width of micro-cracks obtained in Section 4.5 can be expressed as the number of pixels, respectively. Due to different magnification for different images, the actual size that each pixel represents must be calibrated to transfer the pixel of the micro-cracks into metric unit.

5. Results and modeling

5.1. Variation of characteristic parameters of micro-cracks with the strain

The characteristic parameters of the micro-cracks in each SEM image, which was taken under different strain level, are obtained by the procedure mentioned in Section 4. Fig. 8 describes the variation of the number, length and width of micro-cracks on the coating layer with the strain, respectively.

From Fig. 8, it is found that the lengths of the micro-cracks are almost unchanged during deformation, while the number or width of the micro-cracks on the fiber surface varies with the strain. They can be described by polynomial fittings as follows:

$$\begin{aligned} N(\varepsilon) &= 967513\varepsilon^5 - 606104\varepsilon^4 + 152692\varepsilon^3 - 18967\varepsilon^2 + 1173.5\varepsilon\,(\mu\text{m}) \\ W(\varepsilon) &= 305.11\varepsilon^3 - 146.99\varepsilon^2 + 23.565\varepsilon\,(\mu\text{m}) \\ L' &= 15.6\,(\mu\text{m}) \end{aligned} \tag{3}$$

where N and W are the number and width of the micro-cracks, respectively. The average length of micro-cracks can be measured directly from SEM images because the length of the cracks varies slightly during deformation. However, considering that the actual micro-cracks are three-dimensional, while the information on the micro-cracks was obtained from a 2D image, therefore, the crack length need to be modified by match it with a corresponding value in three-dimension. The modified crack length is 16.2 μm.

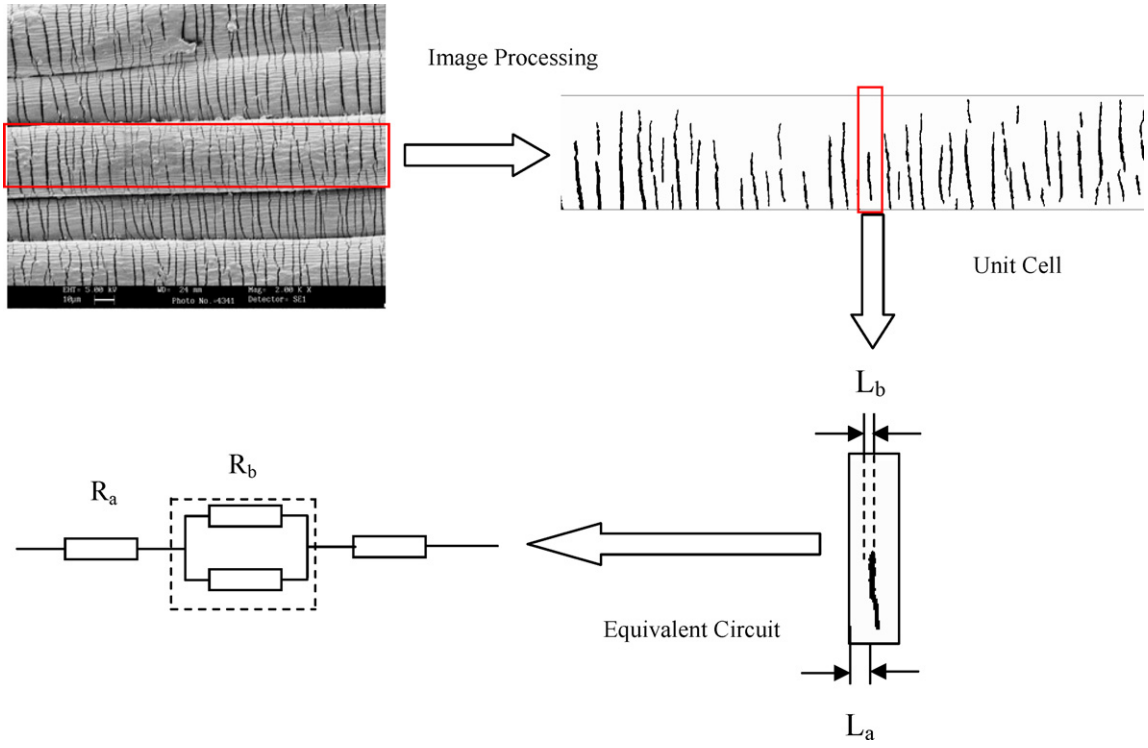

Fig. 9. Flow chart for calculation of equivalent resistance.

5.2. Modeling

For electrically conductive fibers, the electrical resistance can be determined from the resistivity, ρ, the cross-sectional area, A, and the length of the conductor, L, by the relationship:

$$R = \rho\frac{L}{A} \tag{4}$$

where ρ is the resistivity of the electrically conductive fibers. Its value is affected by the resistivity of conductive polymer ρ_p and the characteristics of the coating layer. Because of the large number of micro-cracks on the fiber surface (as shown in Fig. 3), the characteristics of the coating layer will change, leading to the variation in the electrical conductivity when the fiber is extended.

In the followings, we will evaluate the micro damage and investigate the influence of the micro-cracks on resistance of the electrically conductive coating layer. Before the fiber is extended, the resistance of conductive coating layer is

$$R = \rho_p\frac{L_u}{\pi dt} \tag{5}$$

where ρ_p is the resistivity of the conductive polymer PPy and it is a intrinsic material property; L_u and d are the length and the diameter of the PPy-coated Lycra fiber, respectively; t is the thickness of the conductive coating. After loading, both L_u and d vary with the deformation. They can be expressed as

$$L_u = L_0(1+\varepsilon) \tag{6}$$

$$d = d_0(1-\nu\varepsilon) \tag{7}$$

$$t = t_0(1-\nu\varepsilon) \tag{8}$$

where L_0, d_0, and t_0 are the initial length, diameter and thickness, respectively. ν is the Poisson's ratio and ε is applied strain.

Observing the fiber surface shown in Fig. 9, electrically conductive path on the fiber surface is divided into many small elements by micro-cracks and these elements are connected in series. Each element can be treated as an equivalent resistance. The corresponding equivalent circuit of a representation unit is also drawn in Fig. 9. R_a stands for the resistance of no-crack region, while the equivalent resistance of the crack region is represented by R_b.

Considering a single PPy-coated fiber, the surface resistance is expressed as N equivalent resistances R_b and $N+1$ equivalent resistance R_a in series (N is the number of micro-cracks). So the whole resistance of a PPy-coated fiber is

$$R = (N+1)R_a + NR_b \tag{9}$$

In Eq. (9) the resistance of the no-crack region, R_a, can be derived from Eq. (5):

$$R_a = \rho_p\frac{L_a}{\pi t_0 d_0(1-\nu\varepsilon)^2} \tag{10}$$

where L_a is the length of no-crack region in the selected area shown in Fig. 9. The equivalent resistance in parallel connection, R_b, can be expressed as

$$R_b = \rho_p\frac{L_b - W(\varepsilon)}{t_0[\pi d_0(1-\nu\varepsilon) - 2L'](1-\nu\varepsilon)} \tag{11}$$

where L_b is the crack length shown in Fig. 9, and then L' is the average length of the micro-cracks which can be obtained by Section 5.1.

Substituting R_a and R_b in Eq. (10) and Eq. (11) into Eq. (9) and simplifying it, the resistance of electrically conductive fiber can be expressed as

$$R = \frac{\rho_p}{t_0(1-\nu\varepsilon)}\left[\frac{L_0(1+\varepsilon) - N(\varepsilon)\cdot W(\varepsilon)}{\pi d_0(1-\nu\varepsilon)} + \frac{N(\varepsilon)\cdot W(\varepsilon)}{\pi d_0(1-\nu\varepsilon) - 2L'}\right] \tag{12}$$

Considering

$$R_0 = \rho_p\cdot\frac{L_0}{A_0} = \rho_p\cdot\frac{L_0}{\pi d_0 t_0} \tag{13}$$

hence

$$\frac{R}{R_0} = \left[\frac{L_0(1+\varepsilon) - N(\varepsilon)\cdot W(\varepsilon)}{\pi d_0(1-\nu\varepsilon)} + \frac{N(\varepsilon)\cdot W(\varepsilon)}{\pi d_0(1-\nu\varepsilon) - 2L'}\right]\cdot\frac{\pi d_0}{L_0(1-\nu\varepsilon)} \tag{14}$$

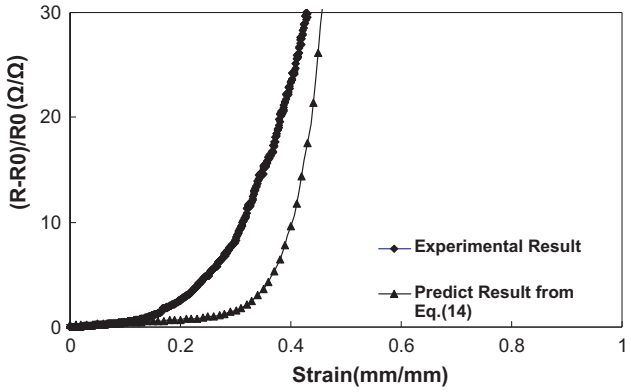

Fig. 10. Comparison of the experimental result and predicted result from Eq. (14).

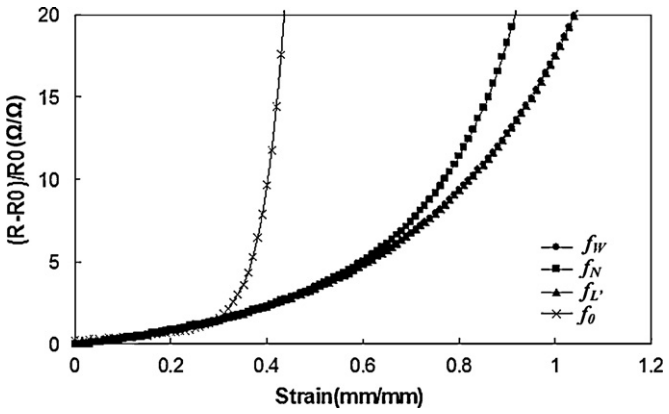

Fig. 11. Sensitivity study.

where N and W are determined by Eq. (3). The initial length and diameter of fibers have been obtained by pixel calibration. L' is the average length of the micro-cracks and the Poisson's ratio ν is 0.4.

6. Discussions

6.1. Comparison of the predicted with the experimental result

The predicted result is compared with the experimental result and is shown in Fig. 10, showing the model can describe the main mechanisms of the strain sensing behavior for PPy-coated Lycra fibers. The difference between the two curves may be resulted from two points: (a) Sample preparation. It is very difficult to make sure that sample was not pre-stretched during sample preparation because Lycra fiber has good elasticity. It can be observed from the microphotographs that the fiber surface had emerged micro-cracks at the beginning of the experiment; (b) Data processing. Statistical method is used in this study to extract characteristic parameters of SEM microphotographs, so the error could not be avoided.

6.2. Sensitivity study

From the analysis above, the variation of resistance is mainly come from the development of the micro-cracks appearing on the coating layer. In order to find the governing parameters among variables, such as the number N, width W and length L' of micro-cracks. Therefore, the study of parameter sensitivity is conducted. In this section, three cases are discussed and for each one only one parameter is kept variable while the other two are taken unchanged, respectively.

Eq. (14) can also be expressed as the function of the electrical resistance and the parameters of micro-cracks. It can be written as

$$f_0 = \frac{R}{R_0} = f(N, W, L') \tag{15}$$

Corresponding the three cases discussed in this section, the dimensionless function f_0 is replaced by f_W, f_N and $f_{L'}$, respectively, and can be expressed as

$$\begin{aligned} f_W &= f(N, W + \Delta W, L') \\ f_N &= f(N + \Delta N, W, L') \\ f_{L'} &= f(N, W, L' + \Delta L') \end{aligned} \tag{16}$$

The three functions are depicted in Fig. 11, where the curves of f_W and $f_{L'}$ coincide. It is found that the influence of the width and length play important role for strain sensing behavior. Two extreme situations can support this judgement. When the cracks length goes through whole perimeter of the fiber, or the width of the crack is large enough, both will lead to conductive path breaking. Therefore, the width and length of micro-cracks are the governing factors in sensing behavior of the PPy-coated fibers.

7. Conclusions

In this paper, the strain sensing behavior of the PPy-coated Lycra fibers are studied experimentally and analytically. The conclusions can be drawn as follows:

(1) The PPy-coated Lycra fiber has good strain sensing behavior during large deformation, even up to the strain of 0.5. The resistance variation of conductive fiber is closely related to the open-close mechanisms of micro-cracks appearing on the coating layer.
(2) The development of micro-cracks during large deformation can be described by the number, width and length of micro-cracks. The relationship between the crack characteristic parameters and the strain is obtained by image processing technique, showing that the length, number and width of micro-cracks affect on the variation of electrical resistance. The width and length of the micro-cracks play important roles for strain sensing behavior.
(3) The resistance variation with the strain can be predicted by the analytical model developed in this study. The agreement between the predicted and the experimental results shows the effectiveness of the model. The model can reflect the main mechanisms of the strain sensing behavior for PPy-coated Lycra fibers.

Acknowledgment

The authors would like to acknowledge the financial supports from National Science Foundation of China under grants 10872168 and 11072202.

References

[1] F. Martinez, G. Obieta, I. Uribe, T. Sikora, E. Ochoteco, Procedia Chemistry 1 (2009) 915–918.
[2] B.J. Munro, T.E. Campbell, G.G. Wallace, J.R. Steele, Sensors and Actuators B 131 (2008) 541–547.
[3] C. Cochrane, V. Koncar, M. Lewandowski, C. Dufour, Sensors 7 (2007) 473–492.
[4] C. Cochrane, M. Lewandowski, V. Koncar, Sensors 10 (2010) 8291–8303.
[5] Y. Xu, F. Jiang, S. Newbern, A. Huang, C.M. Ho, Y.C. Tai, Sensors and Actuators A 105 (2003) 321–329.
[6] C.T. Huang, C.L. Shen, C.F. Tang, S.H. Chang, Sensors and Actuators A 141 (2008) 396–403.
[7] T.E. Campbell, B.J. Munro, G.G. Wallace, J.R. Steele, Journal of Biomechanics 40 (2007) 3056–3059.
[8] W.T. Liu, F. Li, C. Stefanini, D.J. Chen, P. Dario, Robotics and Autonomous Systems 58 (2010) 1138–1148.
[9] D. Kincal, A. Kumar, A.D. Child, J.R. Reynolds, Synthetic Metals 92 (1998) 53–56.

[10] F. Lorussi, A. Tognetti, M. Tesconi, G. Zupone, R. Bartalesi, D. De Rossi, in: C.D. Nugent, al. et (Eds.), Electroactive Fabrics for Distributed, Comfortable and Interactive Systems, Personalised Health Management Systems, IOS Press, 2005.
[11] P. Xue, X.M. Tao, M.Y. Leung, H. Zhang, in: X.M. Tao (Ed.), Wearable Electronics and Photonics, Woodhead Publishing Co., UK, 2005 (Chapter 5).
[12] P. Xue, X.M. Tao, H.Y. Tsang, Applied Surface Science 253 (2007) 3387–3392.
[13] P. Xue, X.M. Tao, T.X. Yu, K.W.Y. Kwork, M.Y. Leung, Textile Research Journal 74 (2004) 929–936.
[14] Z. Chen, B. Cottrell, W. Wong, Engineering Fracture Mechanics 69 (2002) 597–603.
[15] R.C. Gonzalez, R.E. Woods, Digital Image Processing, Second edition, Publishing House of Electronics Industry, Beijing, 2002.
[16] L.T. Mao, R. Xue, L.Q. An, Journal of Chinese Electron Microscopy Society 23 (2004) 579–583 (in Chinese).
[17] C.H. Dong, Z.G. Lai, X.H. Yu (Eds.), Matlab Image Processing and Its Application, National Defense Industry Press, Beijing, 2004 (in Chinese).
[18] Y. Hu, K. Zhang, G.N. Chen, C.W. Wu, Heat Treatment of Metals 30 (2005) 161–163 (in Chinese).
[19] J. Zhang, Study of detection of stress cracks in corn by using acoustic analysis and image analysis, Master's dissertation, Jilin University, 2007 (in Chinese).